catalysts

MDPI

Article

# Catalytic Performance and Characterization of Ni-Co Bi-Metallic Catalysts in *n*-Decane Steam Reforming: Effects of Co Addition

**Qinwei Yu [1], Yi Jiao [1,2], Weiqiang Wang [1], Yongmei Du [1], Chunying Li [1], Jianming Yang [1,*] and Jian Lu [1,*]**

1 State Key Laboratory of Fluorine & Nitrogen Chemicals, Xi'an Modern Chemistry Research Institute, Xi'an 710065, China; qinweiyu204@163.com (Q.Y.); jiaoyiscu@163.com (Y.J.); wqwang07611@163.com (W.W.); dymqw204@sina.com (Y.D.); chunyingli204@163.com (C.L.)

2 Institute of New Energy and Low-Carbon Technology, Sichuan University, Chengdu 610064, China

* Correspondence: yangjm204@163.com (J.Y.); lujian204@263.net (J.L.); Tel.: +86-029-8829-1367 (J.Y.); +86-029-8829-1213 (J.L.)

Received: 29 September 2018; Accepted: 1 November 2018; Published: 5 November 2018


**Abstract:** Co-Ni bi-metallic catalysts supported on Ce-$Al_2O_3$ (CA) were prepared with different Co ratios, and the catalytic behaviors were assessed in the *n*-decane steam reforming reaction with the purpose of obtaining high $H_2$ yield with lower inactivation by carbon deposition. Physicochemical characteristics studies, involving $N_2$ adsorption-desorption, X-ray diffraction (XRD), $H_2$-temperature-programmed reduction ($H_2$-TPR), $NH_3$-temperature-programmed desorption ($NH_3$-TPD), SEM-energy dispersive spectrometer (EDS), and transmission electron microscope (TEM)/HRTEM, were performed to reveal the textural, structural and morphological properties of the catalysts. Activity test indicated that the addition of moderate Co can improve the hydrogen selectivity and anti-coking ability compared with the mono-Ni/Ce-$Al_2O_3$ contrast catalyst. In addition, 12% Co showed the best catalytic activity in the series Co-Ni/Ce-$Al_2O_3$ catalysts. The results of catalysts characterizations of XRD and $N_2$ adsorption-desorption manifesting the metal-support interactions were significantly enhanced, and there was obvious synergistic effect between Ni and Co. Moreover, the introduction of 12% Co and 6% Ni did not exceed the monolayer saturation capacity of the Ce-$Al_2O_3$ support. Finally, 6 h stability test for the optimal catalyst 12%Co-Ni/Ce-$Al_2O_3$ demonstrated that the catalyst has good long-term stability to provide high hydrogen selectivity, as well as good resistance to coke deposition.

**Keywords:** *x*%Co-Ni/Ce-$Al_2O_3$; steam reforming; regeneration; thermal stability; anti-coking ability

## 1. Introduction

Nowadays, hydrogen is recognized as a clean fuel and energy carrier since its combustion produces only water as product [1,2]. However, how to produce hydrogen from primary energy sources (such as hydrocarbons) in an efficient and economic way should be further researched and developed [3–6]. In the past few decades, the most effective approach was catalytic reforming of hydrocarbons. Currently, over 50% of the world's hydrogen supply is from steam reforming of hydrocarbons [7].

Nowadays, $H_2$ is mainly produced by steam reforming of $CH_4$ and other high-energy density liquid fuels, including ethanol, gasoline, diesel, or jet fuel [8–10]. An interesting option is hydrogen production from diesel steam reforming. *n*-decane, one of the main components of diesel, is considered as an ideal source of hydrogen since its availability, easy handling and storage and, relatively high H/C ratio (produce 31 mol of $H_2$ per mole of reacted *n*-decane) [11,12]. However, the *n*-decane

steam reforming reaction is different with $CH_4$, $CH_3OH$, $C_2H_5OH$ etc., and always accompanied by other side effects (cracking, isomerization, hydrogen transfer reaction). More so, the catalysts used in *n*-decane steam reforming reaction are easily to lose activity caused by carbon deposition, especially at higher temperatures [13–15]. Therefore, the catalysts use in *n*-decane steam reforming reaction are put forward higher requirements.

$$C_{10}H_{22} + 20H_2O \rightarrow 31H_2 + 10CO_2$$

Hydrocarbons steam reforming reactions have been extensively investigated over noble and transition metals (Pt, Pd, Rh, Ni, Co, etc.) and several oxide supports ($Al_2O_3$, $CeO_2$, MgO, $ZrO_2$, zeolite, etc.) [16–23], so as to develop excellent catalysts to obtain hydrogen as high yield as possible together with high resistance of coke deposition. Transition metals (especially Ni-based) catalysts, which have the high C–C and C–H bonds breaking activity, have been proved to be very effective for hydrocarbons steam reforming reactions as noble metal catalysts [16–18]. Moreover, the lower cost improved its applicability. Therefore, more and more researchers focused on studying hydrocarbon steam reforming over Ni-based catalysts [16–21]. However, coking is easily deposited on the surface of the active phase Ni, which can lower the catalytic activity [24–27]. Therefore, various promoters were introduced into Ni-based catalysts to improve catalytic activity and coking resistance. Lanthanide metals (La, Ce), alkali metals (Na, K), and alkali earth metals (Mg, Ca, Sr, Ba) promoters [28–33], have been found to be effective for improving coking-resistant capacity. However, the addition of these additives influenced Ni dispersion, due to a part of the promoter is in an intimate contact with nickel [34–36].

In order to improve the anti-coking ability of Ni-based catalyst, and have a slight influence on catalytic activity, many scholars introduced another active metal into Ni-based catalyst to form bi-metallic catalysts [37–42]. Wang et al. [37] introduced Pd into Ni-alumina catalysts, the catalytic activity and stability was obviously improved. Vizcaino et al. [43] found that Cu modified Ni-based catalyst showed better anti-coking ability. The addition of Cu is helpful for the process of eliminating the deposited carbon. In our previous work [44], we have added M (Fe, Co, Cu, Zn) as a promoter into the Ni/Ce-$Al_2O_3$ catalyst in order to improve the anti-coking ability. Clearly, Co doped Ni/Ce-$Al_2O_3$ showed an excellent coking-resistant effect. But, the catalytic activity have a slightly reduction at high temperature (650~800 °C). In another study [45], we added Co as another active species into Ni/Ce-$Al_2O_3$ to form Ni-Co bi-metallic catalyst and investigated the catalytic activity, stability and coking inhibition effect during *n*-decane reforming. The results showed that the introduction of Ni and Co synchronously can effectively suppress carbon deposition and obviously improve catalytic activity. There was obvious synergistic effect between Ni and Co. However, the difference among different Co content on the Co-Ni/Ce-$Al_2O_3$ bi-metallic catalyst has not been discussed. Consequently, it would be valuable to investigate the influence of the content of Ni on *n*-decane steam reforming.

In this paper, the steam reforming experiments of *n*-decane over *x*%Co-Ni/Ce-$Al_2O_3$ catalysts with different Co loading were carried out. The effect of different Co loading on catalytic activity and the amount of deposited carbon were discussed. The purpose of this work is screening the suitable catalysts for steam reforming process in order to maximize *n*-decane conversion and $H_2$ yield, and minimize the formation of byproducts and carbon deposition. This work provided some positive suggestions for catalysts preparation and optimization by studying the structure-activity correlations.

## 2. Results and Discussion

### *2.1. Catalytic Performance*

#### 2.1.1. *n*-Decane Conversion and $H_2$ Selectivity

*n*-decane steam reforming is used as the probe reaction. The initial activity tests over the series catalysts were performed from 650 to 800 °C in order to examine the influence of temperature and

different promoters on catalytic performance. *n*-decane conversion and $H_2$ selectivity are considered the main parameters to check the advantages and disadvantages of the catalysts, and the results are shown in Figure 1a–d. The catalytic activities over these catalysts gradually increase with the temperature. Obviously, the presence of Ni or/and Co can effectively promote the rate of the steam reforming reaction, as well as the selectivity of $H_2$ and *n*-decane conversion. Moreover, the synchronous introduction of Co and Ni further enhanced the catalytic activity compared with the 6%Ni/Ce-$Al_2O_3$(NCA) catalyst. This demonstrates that the addition of Co could provide sufficient Ni active sites for the reactants. In addition, the catalytic activity of *x*%Co-Ni/Ce-$Al_2O_3$ (CNCA) bi-metallic catalysts with different Co content increases firstly and then decreases with Co addition. The catalytic activity reaches the best when the Co content is 12%. This indicated that moderate Co is favor for promoting the activity. There is a synergistic effect between Co and Ni.

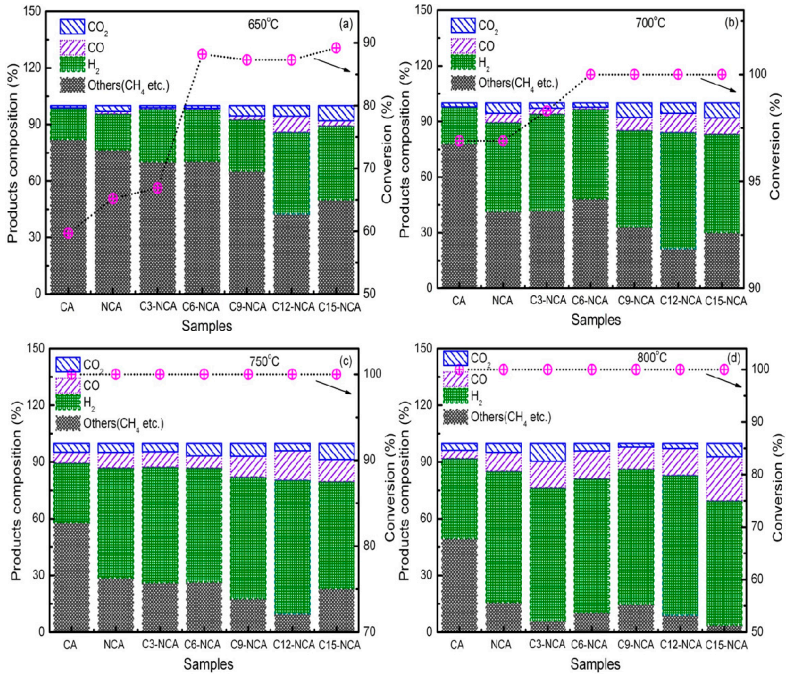


**Figure 1.** *n*-decane conversions and $H_2$ selectivity over the series catalysts at 650 °C (**a**), 700 °C (**b**), 750 °C (**c**), and 800 °C (**d**).

### 2.1.2. Thermal Stability and Regeneration of C12-NCA

To better understand the effect of the ordered co-modification in *n*-decane steam reforming, the 12%Co-Ni/Ce-$Al_2O_3$ (C12-NCA) catalyst was screened out with a 6 h stability test at 750 °C and 800 °C, and the results are displayed in Figure 2a. It can be seen in Figure 2a that the $H_2$ selectivity and *n*-decane conversion have a slightly change within 6 h. The C12-NCA catalyst has a good thermal stability. The C12-NCA catalyst also screened out for regeneration experiment. Carbon deposition on used C12-NCA catalyst was removed by oxygen enriched calcinations at 650 °C. The regenerative C12-NCA catalyst was carried out again in the same reactor as the fresh ones, and the contrast results are presented in Figure 2b. It is found that the *n*-decane conversions and $H_2$ selectivity over the reused-1(-2) C12-NCA catalyst are approximately equal to the results of fresh one. Therefore, the C12-NCA catalyst is renewable.

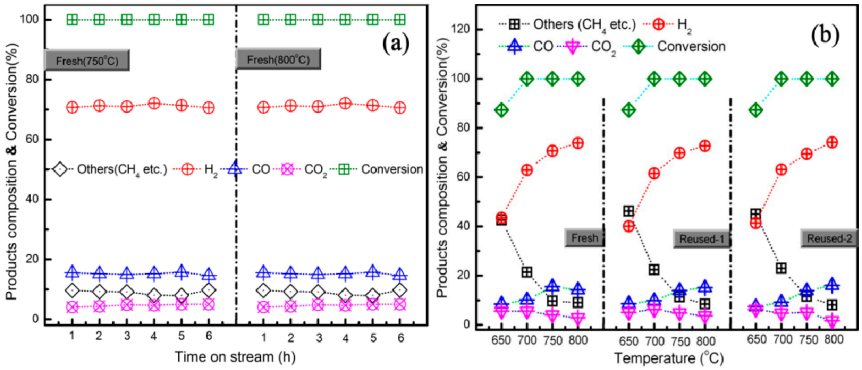


**Figure 2.** Thermal stability (**a**) and regeneration (**b**) over the C12-NCA catalyst.

## 2.2. Fresh Catalyst Characterization

### 2.2.1. $N_2$ Adsorption-Desorption Measurements

Table 1 shows the results of $N_2$ adsorption-desorption results of the fresh and used catalysts. The surface areas of different samples in this work are in the range of similar CA support, even if the introduction of Ni and Co species by impregnation method. The value has a slightly decrease with the addition of Co and Ni, and gradually drops with the increase of Co. The loss can be attributed to the fact that the internal surface area of the CA pore system is progressively covered by Ni, Co species forming a layer [45–47].

**Table 1.** The textural properties of the fresh and used catalysts.

| Catalysts | Textural Properties | | |
|---|---|---|---|
| | Surface Area *($m^2$/g) | Pore Volume (mL/g) | Mean Pore Diameter (nm) |
| CA | 155.9 (69.3) * | 0.49 | 5.42 |
| NCA | 150.2 (83.6) | 0.47 | 5.35 |
| C3-NCA | 149.3 (89.1) | 0.47 | 5.32 |
| C6-NCA | 147.6 (88.6) | 0.47 | 5.34 |
| C9-NCA | 143.9 (92.3) | 0.45 | 5.28 |
| C12-NCA | 140.5 (96.7) | 0.44 | 5.26 |
| C15-NCA | 136.9 (92.4) | 0.44 | 5.26 |

* The numbers in the parentheses represent the surface area of used catalysts.

On the other hand, the surface areas of all catalysts used decrease with different levels after *n*-decane reforming reactions. CA and NCA catalysts decreased by 56% and 44% respectively compared with the fresh ones. Fortunately, the falling range gradually reduced with the addition of Co. Co as the active species showed a better carbon-resistant ability. The results are consistent with the results of the catalyst characterization.

### 2.2.2. X-ray Diffraction (XRD) Analysis

Figure 3 depicts the X-ray diffraction analysis of the fresh CA, NCA and bi-metallic CNCA catalysts. All the samples present similar characteristic features of $\gamma$-$Al_2O_3$ at $2\theta = 45.7°$, 66.8°; cubic fluorite structural $CeO_2$ at $2\theta$ value of 28.5°, 56.3°; and the Ce crystallite at $2\theta = 34.7°$, 49.8° and 59.2° by Bragg's refections [44,48]. For all the catalysts, there was no $CoO_x$, $CoAl_2O_4$, NiO, or $NiAl_2O_4$ diffraction peaks detected. This was probably due to the highly dispersion of $CoO_x$ and NiO particles are not easy to be detected by XRD [49]. Moreover, the synchronous addition of Co and Ni did not form Ni-Co alloy phase. This indicated that active species were strongly interacted with CA support, and all of the as-prepared have a good thermal stability. It also can be seen that the degree of crystallization of all the fresh catalysts are smaller, suggesting that these catalysts are stable at high temperatures,

which is coincides with the surface area analysis [50,51]. This is in agreement with the XRD analysis previously shown and with the observations made in other studies.

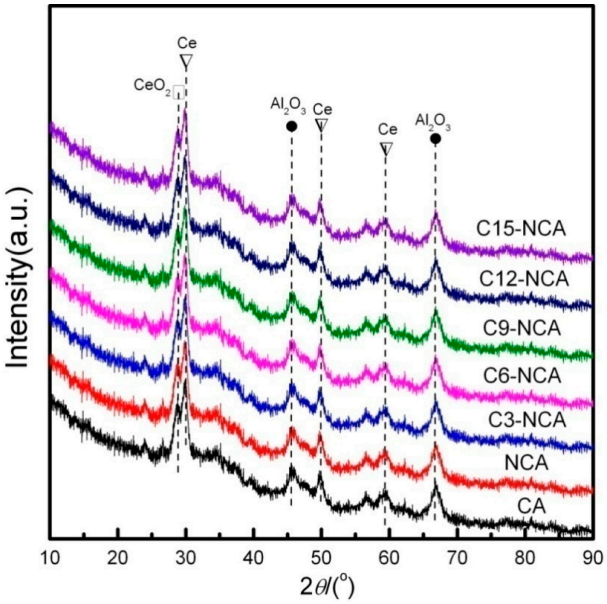


**Figure 3.** X-ray diffraction (XRD) diffraction spectrum of the series catalysts.

### 2.2.3. $H_2$-Temperature-Programmed Reduction ($H_2$-TPR) and $NH_3$-Temperature-Programmed Desorption ($NH_3$-TPD) Analysis

Figure 4 shows the reduction profiles of the CA, and Co, Ni modified CA. It can be seen that there is one or two $H_2$ consumption peaks for CA support at the region of 250~350 °C, which could be assigned to the reduction of a small amount of $CeO_2$ to $CeO_x$ [28,29]. For NCA catalyst, reduction peaks of ~460 °C and ~823 °C which are attributed to the reduction of NiO and $NiAl_2O_4$ [40]. The highest reduction temperature is between 780 and 900 °C indicate the existence of species of NiO with strong interaction with $Al_2O_3$, resulting from the formation of the $NiAl_2O_4$ [42]. For CNCA catalysts with different Co loading, two reduction peaks around ~300 °C and ~610 °C are ascribed to the reduction of $Co_2O_3$ and CoO, respectively [41]. Significantly, the reduction temperatures differences of NiO and $Co_2O_3$ between these CNCA catalysts can be attributed to the existence of different interaction between Co and Ni. It is noteworthy that Co addition can obviously promote the reduction of NiO, and reach the optimal effect at 12% Co loading. There was obvious synergistic effect between Ni and Co, which is consistent with the results of the work reported by Jiao et al. [48,52–56].

$NH_3$-TPD technology was used to investigate the acidities of the series catalysts, such as total amount, nature, and strength distribution, in order to look for the possible interpretation for the above experimental results, and the profiles are shown in Figure 5. The area of desorption peak goes hand in hand with the total amount of surface acid sites, while the peak temperature is closely related to the strength of individual acid site. The peak temperature in the range of 80 to 200 °C is regarded as weak acid sites, and the desorption temperature between 200 to 400 °C is considered the medium acid sites, while the peak temperature locates at 400 to 700 °C corresponds to strong acid sites. Figure 5 shows that CA and NCA catalysts have three desorption peaks at the region of 100~500 °C, which is regarded as the desorption peak of the weak and medium acid. Moreover, all the Co doped NCA catalysts have one strong desorption peak at 100~400 °C. Obviously, the desorption peak temperature moves to a low temperature area by adding Co, suggesting that the amount of acid sites decrease with the introduction of Co. In our previous studies [12,18], we found that the larger acidity and active strong acid centers are easy to give rise to rapid deactivation of the catalyst due to carbon deposition. It is noteworthy that the addition of Co modifier increases the basicity of the NCA catalyst. This process

will result in preventing alkenes further reacting into aromatic or heavier products, which is beneficial to reduce the carbon deposition over catalysts and prolong the work life of catalysts.

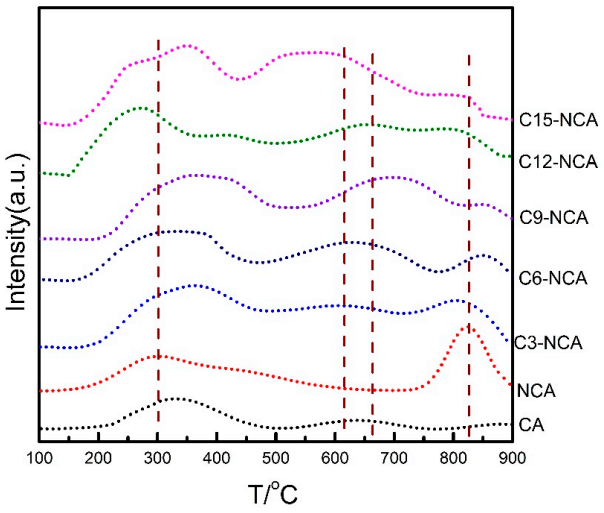


**Figure 4.** $H_2$-temperature-programmed reduction ($H_2$-TPR) results of the series catalysts.

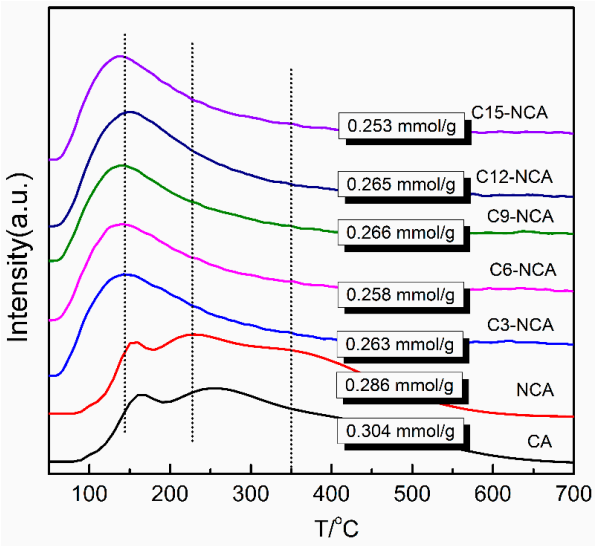


**Figure 5.** $NH_3$-temperature-programmed desorption ($NH_3$-TPD) results of the series catalysts.

### 2.2.4. Transmission Electron Microscope (TEM) Analysis

In this work, the catalytic activity over the C12-NCA catalyst is better than C15-NCA. However, there is somewhat different texture and structural properties between the two. In order to further study the difference between C12-NCA and C15-NCA, the TEM analysis was used to find the influence of microscopic appearance and dispersion on catalytic activity. Figure 6 shows TEM images and Ni or/and Co particle size distributions of C12-NCA and C15-NCA catalysts. It is found that the Ni or/and Co particle size over C12-NCA is mainly focused on 11–20 nm, while the value for C15-NCA is about 16–25 nm. The average particle size of Ni or/and Co of C15-NCA is significantly larger than C12-NCA. Obviously, poor Ni or/and Co distribution over C15-NCA are observed. It may be the reason of the weaker catalytic activity of C15-NCA catalyst. The results indicate that 6% Ni and 15% Co loading is easy to aggregate after 800 °C calcination, which may be due to redundant Co enriching on the catalyst surface and exceed the monolayer saturation capacity of the CA support.

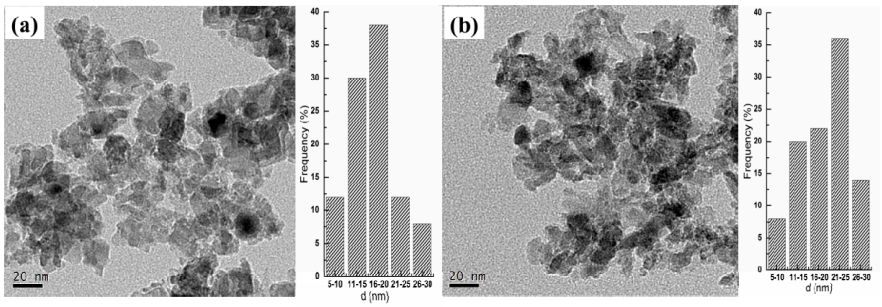


**Figure 6.** Transmission electron microscope (TEM) micrographs of the C12-NCA (**a**) and C15-NCA (**b**) catalysts.

In order to further understand the Ni dispersion, the energy dispersive spectrometer (EDS) mappings of C12-NCA and C15-NCA catalysts were examined. As shown in Figure 7, the red sections correspond to Co, the blue sections correspond to Ce, the green sections correspond to Ni, while the yellow sections correspond to Al. Obviously, Ni and Co particles evenly dispersed on the surface of the CA support over C12-NCA. However, some regions overlap each other for C15-NCA. This may be caused by the partial sintering of 6% Ni and 15% Co loading, and form bigger crystallite and lower metal dispersion. Poor nickel dispersion not only notably impact the physiochemical properties of the catalyst, but also impact the catalytic performance in steam reforming of reactions. Therefore, the dispersion state of active species is one of the main reasons of the activity difference among these catalysts.

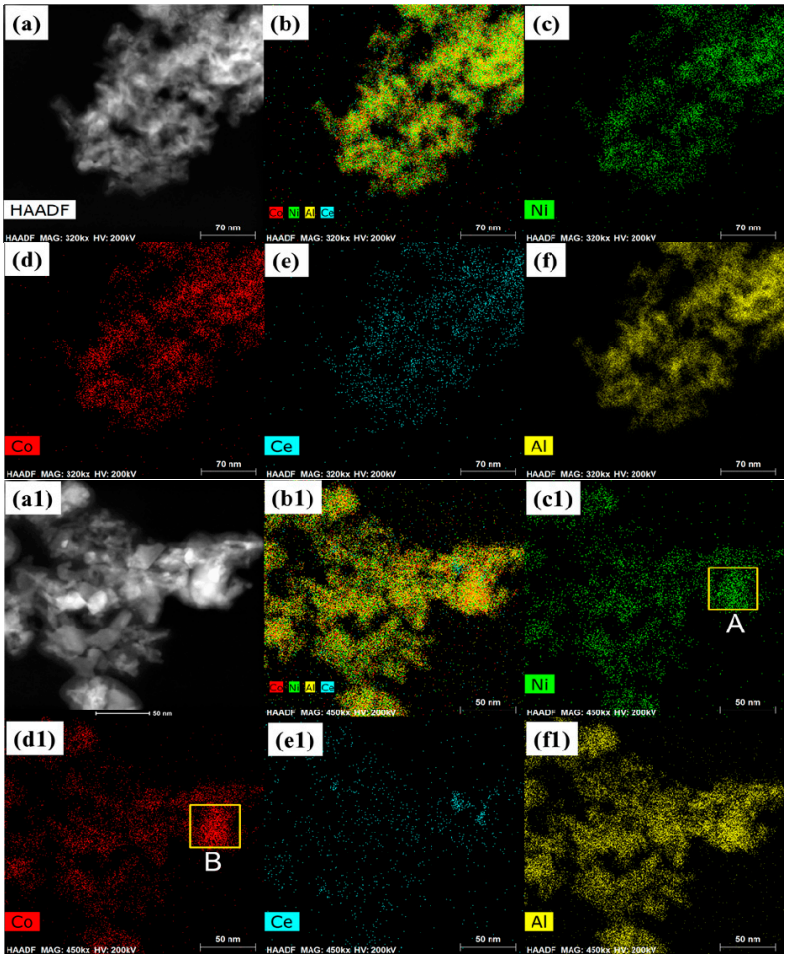


**Figure 7.** Energy dispersive spectrometer (EDS) mappings of the C12-NCA and C15-NCA catalysts. (**a**–**f**) belongs for C12-NCA catalyst; (**a1**–**f1**) belongs for C15-NCA catalyst.

### 2.3. Carbon Deposition

Table 2 presented the amount of carbon deposition over the series catalysts determined by the temperature programmed oxidation (TPO)-infrared spectrum (IR) analysis. It can be seen that the amount of carbon deposition is varied with the introduction of Ni and Co. Clearly, the amount of carbon deposition over CA catalyst is larger than others, and the values drop off with the Co content increased. For the bi-metallic C12(C15)-NCA catalyst, the amount of carbon deposition (<4.0 mg/g-fuel) is much less than conventional Ni-alumina catalysts. The possible reasons are that the addition of Co reduces the acidity of the CA catalyst and carbon dioxide adsorption, and decreases carbon deposition generation during *n*-decane steam reforming process [48]. According to the literature [57], Co addition can increase the dispersion state of Ni, prevent metal sintering, and inhibit carbon deposition, which is consistent with our results in this work.

**Table 2.** The amount of carbon deposition over used catalysts.

| Catalysts | Carbon Deposition | |
|---|---|---|
| | [mg/($g_{Cat}$·h)] | [mg/g$C_{Feed}$] |
| CA | 258.9 | 11.6 |
| NCA | 194.3 | 8.55 |
| C3-NCA | 178.8 | 7.87 |
| C6-NCA | 143.2 | 6.30 |
| C9-NCA | 114.1 | 5.02 |
| C12-NCA | 88.6 | 3.90 |
| C15-NCA | 75.0 | 3.30 |

### 2.4. Used Catalyst Characterization

The formation of carbon deposition on the used catalyst was also evidenced by SEM observations. In Figure 8a–g, the micrographs of used catalysts are presented. Carbon deposition grows on the surface of catalysts in different range. It is observed from Figure 8h that the Ni species is occupied at the tip of the filamentous carbon and the Ni metal particle size is found to be ca. 30 nm. This can demonstrate that active metal has removed from the surface of catalyst with the generation of filamentous carbon. The results are consistent with the mechanisms of filamentous carbon growth in literature [58]. In addition, the C content over the used CA, NCA, C3-NCA, C6-NCA, C9-NCA, C12-NCA, C15-NCA catalysts are 91.14%, 63.90%, 56.46%, 49.89%, 34.79%, 14.94% and 8.31%, respectively. It clearly indicates that the C content over the used catalysts has a close relationship with the surface area. Obviously, the Brunauer–Emmett–Teller (BET) specific surface area decrease caused by the formation of the carbon deposition is another main reason of the activity difference among these catalysts.

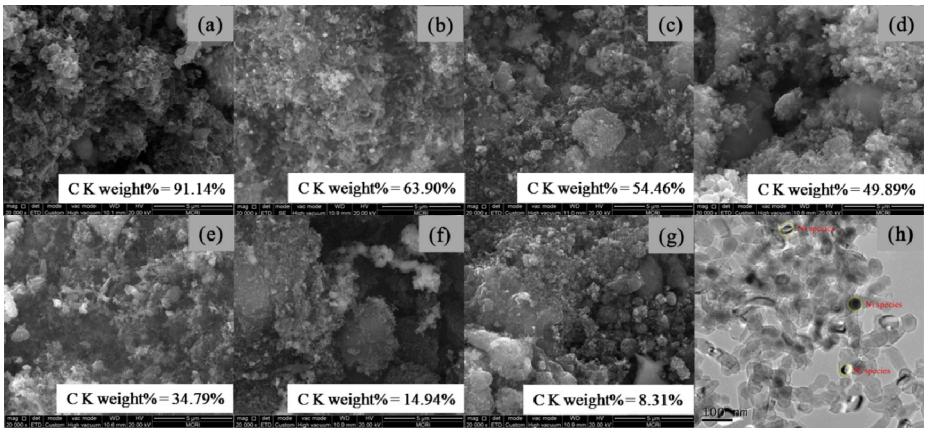


**Figure 8.** Field emission scanning electron microscopy (FESEM) micrographs of the used catalysts: CA (**a**), NCA (**b**), C3-NCA (**c**), C6-NCA (**d**), C9-NCA (**e**), C12-NCA (**f**), C15-NCA (**g**) and C15-NCA (**h**).

## 3. Experimental Section

### *3.1. Catalysts Preparation*

Ce-$Al_2O_3$ composite oxides (5 wt.% Ce) support was prepared by coprecipitation method, and the complete experimental procedure is detailed in references [8,44]. The catalysts were prepared by incipient wetness impregnation using $Ni(NO_3)_2{\cdot}6H_2O$ and $Co(NO_3)_2{\cdot}6H_2O$ as the precursors of Ni and Co, respectively. After impregnation and drying (120 °C, 3 h), the samples were calcined in air at 800 °C for 4 h. Finally, the mono-metallic Ni catalyst (Ni/Ce-$Al_2O_3$, 6 wt.% Ni), and Co-Ni bi-metallic catalysts {Co-Ni/Ce-$Al_2O_3$, 6 wt.% Ni, *x* wt.% Co (*x* = 3, 6, 9, 12, 15)} were made into columnar particles (length of 5 mm, diameter of 5 mm), and marked as NCA, C3-NCA, C6-NCA, C9-NCA, C12-NCA and C15-NCA, respectively.

### *3.2. Catalysts Characterization*

Surface area and pore volume were obtained from $N_2$ adsorption-desorption isotherms at 77 K performed on a Quanta chrome autosorb-1 analyzer. Before analysis, the samples were dried at room temperature and then vacuum degassed at 300 °C for 5 h. X-ray diffraction (XRD) patterns were obtained on a Bruker D8 Advance diffractometer with a copper Kα radiation source operated at 40 kV and 40 mA. During the analysis, the catalysts were scanned from 20° to 80° at a speed of 5 °/min. Furthermore, temperature-programmed reduction (TPR) profiles of fresh catalysts under $H_2$-blanket were carried out using a TP-5076 TPR instrument. The samples (100 mg) were heated to 400 °C at a heating rate of 8 °C/min in a flow of Ar, kept for 45 min, and then cooled to 30 °C. The flow gas was switched to $H_2$ (5%) in Ar (25 mL/min). The reduction was carried out from 30 °C to 920 °C, at a heating rate of 8 °C/min. $NH_3$-temperature-programmed desorption ($NH_3$-TPD) experiments were performed in a TP-5076 TPD instrument (Tian Jin Xian Quan Instrument Co., Ltd., Tianjin, China) equipped with a thermal conductivity detector (TCD) to investigate the surface acidity of catalysts. Prior to analysis, catalysts were pretreated at 400 °C for 1 h in a flow of $N_2$ to clean the catalyst surface and then cooled to room temperature. After the pretreatment, a 2% $NH_3/N_2$ gas mixture was passed through the sample at 20 mL/min and the temperature was raised from 50 to 750 °C at a heating rate of 8 °C/min. In addition, morphological characterization was examined by field emission scanning electron microscopy (FESEM) using a Quanta 600FEG Field emission scanning electron microscope (FEI, Hillsboro, OR, USA) and coupled with Oxford-IE-250 energy dispersive spectrometer (EDS) for local elemental composition determination.

Transmission electron microscope (TEM) analysis was obtained using a FEI titan themis 200 transmission electron microscope (FEI, Hillsboro, OR, USA) equipped with Bruker super-X energy-dispersive spectrometer (EDS). Prior to measurement, the samples were dispersed in ethanol at first and then collected on a Cu grid which was covered with carbon film.

### *3.3. Catalytic Performance Test*

*n*-decane steam reforming reaction was carried out in a fixed-bed stainless steel tubular reactor (i.d. = 12 mm) at atmospheric pressure. 3.0 g catalyst diluted with equi-volume quartz particles was charged for each catalytic assessment. The schematic diagram was shown in Figure 9. In each run, water and *n*-decane were pre-mixed quantitatively at 350 °C and the mixture vapor was fed into the reactor. The volumetric feed flow of water and *n*-decane are both 2.5 mL/min. The reactor was set at 650 °C, 700 °C, 750 °C or 800 °C respectively for evaluating the catalysts' activity.

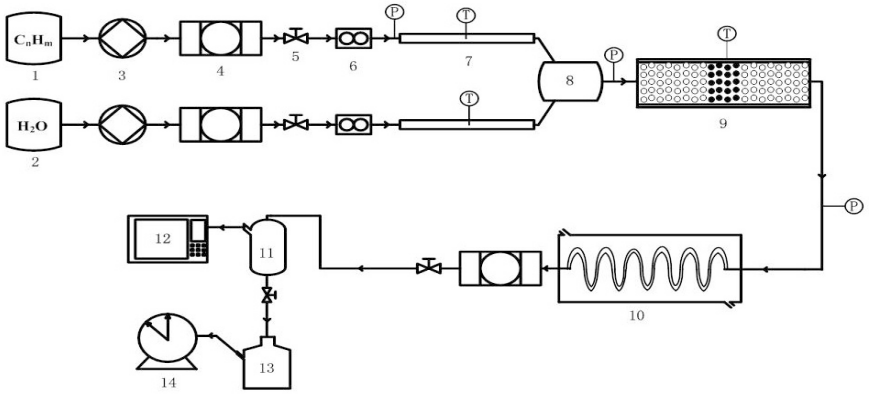


**Figure 9.** Schematic diagram of apparatus. 1-feed tank; 2-water tank; 3-high pressure metering pump; 4-filter; 5-check valve; 6-mass flow meter; 7-heating system; 8-mixer; 9-reactor; 10-cold trap; 11-gas-liquid separator; 12-gas chromatograph; 13-liquid receiver; 14-wet gas flow meter.

The reaction effluents were on-line analyzed by Gas Chromatography with FID detector (GC-2010, SHIMADZU Co., Ltd., Kyoto, Japan) equipped with HP-Al/S separation capillary column ($CH_4$, $C_2H_4$, $C_2H_6$, $C_3H_8$, $C_3H_6$, $C_4$); and TCD detector with TDX-01 packed column ($H_2$, CO and $CO_2$). Solid products deposited covering the catalysts were investigated by temperature programmed oxidation (TPO), and the characteristics signals of CO and $CO_2$ were tested by IR analyzer.

Activity data were reported as *n*-decane conversion $X_A$ (%), and $H_2$, CO and $CO_2$ selectivity ($S_i$), which are defined as follows:

$$X_A(\%) = \frac{\Delta m_A}{m_{A,in}} = \frac{m_{A,in} - m_{A,out}}{m_{A,in}} \times 100 \quad (1)$$

$$S_i = \frac{moles P_i}{\sum_{i=1}^{n} moles P_i} \times 100\% \quad (2)$$

where *i* represents the different gas products detected.

## 4. Conclusions

Series Co-Ni bi-metallic catalysts supported on Ce-$Al_2O_3$ (CA) with different Co ratios are prepared for *n*-decane steam reforming towards $H_2$ preparation, so as to screen appropriate Co content. $N_2$ adsorption-desorption, XRD, $NH_3$-TPD, SEM-EDS, and TEM were used to explain the relationship between catalytic activity and textural-structure properties, microscopic appearance and dispersion state of the catalysts. The activity test indicated that the addition of Co resulted in higher selectivity of hydrogen compared with NCA contrast catalyst. The results indicated that 12% Co showed better hydrogen selectivity (74%), *n*-decane conversion (100%), and anti-carbon ability (3.90 mg/g-fuel). Moreover, thermal stability and regeneration performance were also tested, and the results showed that reforming activity over C12-NCA catalyst was stable in 6 h, and the hydrogen selectivity and *n*-decane conversion over regenerated catalysts were almost close to the fresh ones.

The results were mainly interpreted on the basis of characterization studies, which revealed the significant role of textural and structural properties, microscopic appearance and dispersion state on reforming performance. Obviously, the dispersion state and the BET-specific surface area decrease caused by the formation of the carbon deposition are the main reasons for the activity difference among these catalysts.

**Author Contributions:** Q.Y., Y.J. and J.L. conceived and designed the experiments; Q.Y. and Y.J. performed the experiments; W.W., Y.D. and C.L. contributed with catalyst characterization; J.Y. analyzed the data; J.L. administrated the project; Q.Y. wrote original draft; Q.Y. and Y.J. reviewed and modified the manuscript.

**Funding:** The research was funded by the special program for Key Basic Research in China (Grant No. 0040202204) and the Key Research& Development Plan in Shaanxi Province (2017ZDXM-GY-042, 2017ZDXM-GY-070).

**Conflicts of Interest:** The authors declare no conflict of interest.

## References


1. Cheekatamarla, P.K.; Finnerty, C.M. Reforming catalysts for hydrogen generation in fuel cell applications. *J. Power Sources* **2006**, *160*, 490–499. [CrossRef]
2. Kaewpanha, M.; Guan, G.; Hao, X.; Wang, Z.; Kasai, Y.; Kakuta, S.; Kusakabe, K.; Abudula, A. Steam reforming of tar derived from the steam pyrolysis of biomass over metal catalyst supported on zeolite. *J. Taiwan Inst. Chem. Eng.* **2013**, *44*, 1022–1026. [CrossRef]
3. Liu, X.; Yang, X.; Liu, C.; Chen, P.; Yue, X.; Zhang, S. Low-temperature catalytic steam reforming of toluene over activated carbon supported nickel catalysts. *J. Taiwan Inst. Chem. Eng.* **2016**, *65*, 233–241. [CrossRef]
4. Yang, R.X.; Chuang, K.H.; Wey, M.Y. Hydrogen production through methanol steam reforming: Effect of synthesis parameters on Ni-Cu/CaO-$SiO_2$ catalysts activity. *Int. J. Hydrog. Energy* **2014**, *39*, 19494–19501. [CrossRef]
5. Oararteta, L.; Remiro, A.; Aguayo, A.T.; Bilbao, J.; Gayubo, A.G. Effect of operating conditions on dimethyl ether steam reforming over a $CuFe_2O_4$/γ-$Al_2O_3$ bifunctional catalyst. *Ind. Eng. Chem. Res.* **2015**, *54*, 9722–9732. [CrossRef]
6. Dou, B.; Song, Y.; Wang, C.; Chen, H.; Xu, Y. Hydrogen production from catalytic steam reforming of biodiesel byproduct glycerol: Issues and challenges. *Renew. Sust. Energy Rev.* **2014**, *30*, 950–960. [CrossRef]
7. Chen, H.; Ding, Y.; Cong, N.T.; Dou, B.; Dupont, V.; Ghadiri, M.; Williams, P.T. Progress in low temperature hydrogen production with simultaneous $CO_2$ abatement. *Chem. Eng. Res. Des.* **2011**, *89*, 1774–1782. [CrossRef]
8. Jiao, Y.; Sun, D.; Zhang, J.; Du, Y.; Kang, J.; Li, C.; Lu, J.; Wang, J.; Chen, Y. Steam reforming of *n*-decane toward $H_2$ production over Ni/Ce-$Al_2O_3$ composite catalysts: Effects of M (M = Fe, Co, Cu, Zn) promoters. *J. Anal. Appl. Pyrol.* **2016**, *120*, 238–246. [CrossRef]
9. Dan, M.; Mihet, M.; Tasnadi-Asztalos, Z.; Imre-Lucaci, A.; Katona, G.; Lazar, M.D. Hydrogen Production by Ethanol Steam Reforming on Nickel Catalysts: Effect of Support Modification by $CeO_2$ and $La_2O_3$. *Fuel* **2015**, *147*, 260–268. [CrossRef]
10. Bambal, A.S.; Vecchio, K.S.; Cattolica, R.J. Catalytic effect of Ni and Fe addition to gasifier bed material in the steam reforming of producer gas. *Ind. Eng. Chem. Res.* **2014**, *53*, 13656–13666. [CrossRef]
11. Sangjun, Y.; Youngchan, C.; Jaegoo, L. Hydrogen production from biomass tar by catalytic steam reforming. *Energy Convers. Manag.* **2010**, *51*, 42–47.
12. Jiao, Y.; Du, Y.; Zhang, J.; Li, C.; Xue, Y.; Lu, J.; Wang, J.; Chen, Y. Steam reforming of *n*-decane for $H_2$ production over Ni modified La-$Al_2O_3$ catalysts: Effects of the active component Ni content. *J. Anal. Appl. Pyrol.* **2015**, *116*, 58–67. [CrossRef]
13. Dieuzeide, M.L.; Laborde, M.; Amadeo, N.; Cannilla, C.; Bonura, G.; Frusteri, F. Hydrogen production by glycerol steam reforming: How Mg doping affects the catalytic behaviour of Ni/$Al_2O_3$ catalysts. *Int. J. Hydrog. Energy* **2016**, *41*, 157–166. [CrossRef]
14. Sun, L.Z.; Tan, Y.S.; Zhang, Q.D.; Xie, H.J.; Song, F.E.; Sun, Y.Z. Effects of $Y_2O_3$-modification to Ni/γ-$Al_2O_3$ catalysts on auto thermal reforming of methane with $CO_2$ to syngas. *Int. J. Hydrog. Energy* **2013**, *38*, 1892–1900. [CrossRef]
15. Quitete, C.P.B.; Bittencourt, R.C.P.; Souza, M.M.V.M. Coking resistance evaluation of tar removal catalysts. *Catal. Commun.* **2015**, *71*, 79–83. [CrossRef]
16. Rossetti, I.; Biffi, C.; Bianchi, C.L.; Nichele, V.; Signoretto, M.; Menegazzo, F.; Finocchio, E.; Ramis, G.; Di Michele, A. Ni/$SiO_2$ and Ni/$ZrO_2$ catalysts for the steam reforming of ethanol. *Appl. Catal. B Environ.* **2012**, *117*, 384–396. [CrossRef]
17. Mondal, T.; Pant, K.K.; Dalai, A.K. Catalytic oxidative steam reforming of bio-ethanol for hydrogen production over Rh promoted Ni/$CeO_2$-$ZrO_2$ catalyst. *Int. J. Hydrog. Energy* **2015**, *40*, 2529–2544. [CrossRef]
18. Jiao, Y.; Zhang, J.; Du, Y.; Li, F.; Li, C.; Lu, J.; Wang, J.; Chen, Y. Hydrogen production by catalytic steam reforming of hydrocarbon fuels over Ni/Ce-$Al_2O_3$, bifunctional catalysts: Effects of SrO addition. *Int. J. Hydrog. Energy* **2016**, *41*, 13436–13447. [CrossRef]
19. Bizkarra, K.; Barrio, V.L.; Yartu, A.; Requies, J.; Arias, P.L.; Cambra, J.F. Hydrogen production from *n*-butanol over alumina and modified alumina nickel catalysts. *Int. J. Hydrog. Energy* **2015**, *40*, 5272–5280. [CrossRef]

20. Souza, G.D.; Marcilio, N.R.; Perezlopez, O.W. Dry reforming of methane at moderate temperatures over modified Co-Al Co-precipitated catalysts. *Mater. Res.* **2014**, *17*, 1047–1055. [CrossRef]
21. Huang, L.; Chong, C.; Chen, L.; Wang, Z.; Zhong, Z.; Campos-Cuerva, C.; Lin, J. Monometallic carbonyl-derived $CeO_2$-supported Rh and Co bicomponent catalysts for CO-Free, high-yield $H_2$ generation from low-temperature ethanol steam reforming. *ChemCatChem* **2013**, *5*, 220–234. [CrossRef]
22. Liguras, D.K.; Kondarides, D.I.; Verykios, X.E. Production of hydrogen for fuel cells by steam reforming of ethanol over supported noble metal catalysts. *Appl. Catal. B Environ.* **2003**, *43*, 345–354. [CrossRef]
23. Cavallaro, S. Ethanol steam reforming on $Rh/Al_2O_3$ catalysts. *Energy Fuels* **2000**, *14*, 1195–1199. [CrossRef]
24. Wang, Z.; Wang, C.; Chen, S.; Liu, Y. Co-Ni bimetal catalyst supported on perovskite-type oxide for steam reforming of ethanol to produce hydrogen. *Int. J. Hydrog. Energy* **2014**, *39*, 5644–5652. [CrossRef]
25. De Lima, S.M.; da Cruz, I.O.; Jacobs, G.; Davis, B.H.; Mattos, L.V.; Noronha, F.B. Study of catalyst deactivation and reaction mechanism of steam reforming, partial oxidation, and oxidative steam reforming of ethanol over $Co/CeO_2$ catalyst. *J. Catal.* **2009**, *268*, 268–281. [CrossRef]
26. Frusteri, F.; Freni, S.; Spadaro, L.; Chiodo, V.; Bonura, G.; Donato, S.; Cavallaro, S. $H_2$ production for MC fuel cell by steam reforming of ethanol over MgO supported Pd, Rh, Ni and Co catalysts. *Catal. Commun.* **2004**, *5*, 611–615. [CrossRef]
27. Freni, S.; Cavallaro, S.; Mondello, N.; Spadaro, L.; Frusteri, F. Production of hydrogen for MC fuel cell by steam reforming of ethanol over MgO supported Ni and Co catalysts. *Catal. Commun.* **2003**, *4*, 259–268. [CrossRef]
28. Ashok, J.; Kawi, S. Steam reforming of toluene as a biomass tar model compound over $CeO_2$ promoted $Ni/CaO-Al_2O_3$ catalytic system. *Int. J. Hydrog. Energy* **2013**, *38*, 13938–13949. [CrossRef]
29. Tao, J.; Zhao, L.Q.; Dong, C.Q.; Qiang, L.; Du, X.Z.; Dahlquist, E. Catalytic steam reforming of toluene as a model biomass gasification tar compound using $Ni-CeO_2$/SBA-15 catalysts. *Energies* **2013**, *6*, 3284–3296. [CrossRef]
30. Guan, G.; Chen, G.; Kasai, Y.; Lim, E.W.C.; Hao, X.; Kaewpanha, M.; Abuliti, A.; Fushimi, C.; Tsutsumi, A. Catalytic steam reforming of biomass tar over iron- or nickel-based catalyst supported on calcined scallop shell. *Appl. Catal. B Environ.* **2012**, *115–116*, 159–168. [CrossRef]
31. Blanco, P.H.; Wu, C.; Onwudili, J.A.; Williams, P.T. Characterization and evaluation of $Ni/SiO_2$ catalysts for hydrogen production and tar reduction from catalytic steam pyrolysis-reforming of refuse-derived fuel. *Appl. Catal. B Environ.* **2013**, *134–135*, 238–250. [CrossRef]
32. Garbarino, G.; Finocchio, E.; Lagazzo, A.; Valsamakis, I.; Riani, P.; Escribano, V.S.; Busca, G. Steam reforming of ethanol-phenol mixture on $Ni/Al_2O_3$: Effect of magnesium and boron on catalytic activity in the presence and absence of sulphur. *Appl. Catal. B Environ.* **2014**, *147*, 813–826. [CrossRef]
33. Koike, M.; Ishikawa, C.; Li, D.; Wang, L.; Nakagawa, Y.; Tomishige, K. Catalytic performance of manganese-promoted nickel catalysts for the steam reforming of tar from biomass pyrolysis to synthesis gas. *Fuel* **2013**, *103*, 122–129. [CrossRef]
34. Chen, X.; Liu, Y.; Niu, G.; Yang, Z.; Bian, M.; He, A. High temperature thermal stabilization of alumina modified by lanthanum species. *Appl. Catal. A Gen.* **2001**, *205*, 159–172. [CrossRef]
35. Oudet, F.; Courtine, P.; Vejux, A. Thermal stabilization of transition alumina by structural coherence with $LnAlO_3$ (Ln = La, Pr, Nd). *J. Catal.* **1988**, *114*, 112–120. [CrossRef]
36. Borowiecki, T.; Denis, A.; Rawski, M.; Gołębiowski, A.; Stołecki, K.; Dmytrzyk, J.; Kotarba, A. Studies of potassium-promoted nickel catalysts for methane steam reforming: Effect of surface potassium location. *Appl. Surf. Sci.* **2014**, *300*, 191–200. [CrossRef]
37. Wang, Y.H.; Zhang, J.C. Hydrogen production on $Ni-Pd-Ce/\gamma-Al_2O_3$ catalyst by partial oxidation and steam reforming of hydrocarbons for potential application in fuel cells. *Fuel* **2005**, *84*, 1926–1932. [CrossRef]
38. Fauteux-Lefebvre, C.; Abatzoglou, N.; Braidy, N.; Achouri, I.E. Diesel steam reforming with a nickel-alumina spinel catalyst for solid oxide fuel cell application. *J. Power Sources* **2011**, *196*, 7673–7680. [CrossRef]
39. Al-Musa, A.A.; Ioakeimidis, Z.S.; Al-Saleh, M.S.; Al-Zahrany, A.; Marnellos, G.E.; Konsolakis, M. Steam reforming of iso-octane toward hydrogen production over mono- and bi-metallic $Cu-Co/CeO_2$ Catalysts: Structure-activity correlations. *Int. J. Hydrog. Energy* **2014**, *39*, 19541–19554. [CrossRef]
40. Ramasamy, K.K.; Gray, M.; Job, H.; Wang, Y. Direct syngas hydrogenation over a Co-Ni bimetallic catalyst: Process parameter optimization. *Chem. Eng. Sci.* **2015**, *135*, 266–273. [CrossRef]

41. Laosiripojana, N.; Sutthisripok, W.; Charojrochkul, S.; Assabumrungrat, S. Development of Ni-Fe bimetallic based catalysts for biomass tar cracking/reforming: Effects of catalyst support and Co-fed reactants on tar conversion characteristics. *Fuel Process. Technol.* **2014**, *127*, 26–32. [CrossRef]
42. Dave, C.D.; Pant, K.K. Renewable hydrogen generation by steam reforming of glycerol over zirconia promoted ceria supported catalyst. *Renew Energy* **2011**, *36*, 3195–3202. [CrossRef]
43. Vizcaíno, A.J.; Carrero, A.; Calles, J.A. Hydrogen production by ethanol steam reforming over Cu-Ni supported catalysts. *Int. J. Hydrog. Energy* **2007**, *32*, 1450–1461. [CrossRef]
44. Jiao, Y.; Zhang, J.; Du, Y.; Sun, D.; Wang, J.; Chen, Y.; Lu, J. Steam reforming of hydrocarbon fuels over M (Fe, Co, Ni, Cu, Zn)-Ce bimetal catalysts supported on $Al_2O_3$. *Int. J. Hydrog. Energy* **2016**, *41*, 10473–10482. [CrossRef]
45. Goula, M.A.; Charisiou, N.D.; Papageridis, K.N.; Delimitis, A.; Pachatouridou, E.; Iliopoulou, E.F. Nickel on alumina catalysts for the production of hydrogen rich mixtures via the biogas dry reforming reaction: Influence of the synthesis method. *Int. J. Hydrog. Energy* **2015**, *40*, 9183–9200. [CrossRef]
46. Bereketidou, O.A.; Goula, M.A. Biogas reforming for syngas production over nickel supported on ceria-alumina catalysts. *Catal. Today* **2012**, *195*, 93–100. [CrossRef]
47. Papageridis, K.N.; Siakavelas, G.; Charisiou, N.D.; Avraam, D.G.; Tzounis, L.; Kousi, K.; Goula, M.A. Comparative study of Ni, Co, Cu supported on γ-alumina catalysts for hydrogen production via the glycerol steam reforming reaction. *Fuel Process. Technol.* **2016**, *152*, 156–175. [CrossRef]
48. Jiao, Y.; He, Z.; Wang, J.; Chen, Y. n-decane steam reforming for hydrogen production over mono- and bi-metallic Co-Ni/Ce-$Al_2O_3$ catalysts: Structure-activity correlations. *Energy Convers. Manag.* **2017**, *148*, 954–962. [CrossRef]
49. Cassinelli, W.H.; Feio, L.S.F.; Araújo, J.C.S.; Hori, C.E.; Noronha, F.B.; Marques, C.M.P.; Bueno, J.M.C. Effect of $CeO_2$ and $La_2O_3$ on the activity of $CeO_2$-$La_2O_3$/ $Al_2O_3$-supported Pd catalysts for steam reforming of methane. *Catal. Lett.* **2008**, *120*, 86–94. [CrossRef]
50. Peña, J.A.; Herguido, J.; Guimon, C.; Monzón, A.; Santamarí, J. Hydrogenation of acetylene over Ni/$NiAl_2O_4$ catalyst: Characterization, coking, and reaction studies. *J. Catal.* **1996**, *159*, 313–322. [CrossRef]
51. Boukha, Z.; Jiménez-González, C.; Rivas, B.D.; González-Velasco, J.R.; Gutiérrez-Ortiz, J.I.; López-Fonseca, R. Synthesis, characterisation and performance evaluation of spinel-derived Ni/$Al_2O_3$ catalysts for various methane reforming reactions. *Appl. Catal. B Environ.* **2014**, *158–159*, 190–201. [CrossRef]
52. Nandini, A.; Pant, K.K.; Dhingra, S.C. $CeO_2$ and Mn-Promoted Ni/$Al_2O_3$ Catalysts for Stable $CO_2$ Reforming of Methane. *Appl. Catal. A Gen.* **2005**, *290*, 166–174. [CrossRef]
53. Xu, G.; Shi, K.; Gao, Y.; Xu, H.; Wei, Y. Studies of Reforming Natural Gas with Carbon Dioxide to Produce Synthesis Gas: The Role of $CeO_2$ and MgO Promoters. *J. Mol. Catal. A Chem.* **1999**, *147*, 47–54. [CrossRef]
54. Siew, K.W.; Lee, H.C.; Gimbun, J.; Cheng, C.K. Production of CO-Rich Hydrogen Gas from Glycerol Gry Reforming over La-promoted Ni/$Al_2O_3$ Catalyst. *Int. J. Hydrog. Energy* **2014**, *39*, 6927–6936. [CrossRef]
55. Zeng, S.H.; Zhang, L.; Zhang, X.H.; Wang, Y.; Pan, H.; Su, H.Q. Modification Effect of Natural Mixed Rare Earths on Co/g-$Al_2O_3$ catalysts for $CH_4$/$CO_2$ Reforming to Synthesis Gas. *Int. J. Hydrog. Energy* **2012**, *37*, 9994–10001. [CrossRef]
56. Djaidja, A.; Libs, S.; Kiennemann, A.; Barama, A. Characterization and Activity in Dry Reforming of Methane on NiMg/Al and Ni/MgO Catalysts. *Catal. Today* **2006**, *113*, 194–200. [CrossRef]
57. Resini, C.; Delgado, M.C.H.; Presto, S.; Alemany, L.J.; Riani, P.; Marazza, R.; Ramis, G.; Busca, G. Yttria-stabilized zirconia (YSZ) supported Ni-Co alloys (precursor of SOFC anodes) as catalysts for the steam reforming of ethanol. *Int. J. Hydrog. Energy* **2008**, *33*, 3728–3735. [CrossRef]
58. Fenelonov, V.B.; Derevyankin, A.Y.; Okkel, L.G.; Avdeeva, L.B.; Zaikovskii, V.I.; Moroz, E.M.; Salanov, A.N.; Rudina, N.A.; Likholobov, V.A.; Shaikhutdinov, S.K. Structure and texture of filamentous carbons produced by methane decomposition on Ni and Ni-Cu catalysts. *Carbon* **1997**, *35*, 1129–1140. [CrossRef]